PANCHROMATIC OBSERVATIONS OF SN 2011dh POINT TO A COMPACT PROGENITOR STAR

A. M. SODERBERG[1], R. MARGUTTI[1], B. A. ZAUDERER[1], M. KRAUSS[2], B. KATZ[3,22], L. CHOMIUK[1,2], J. A. DITTMANN[1], E. NAKAR[4],
T. SAKAMOTO[5,6], N. KAWAI[7], K. HURLEY[8], S. BARTHELMY[9], T. TOIZUMI[7], M. MORII[7], R. A. CHEVALIER[10], M. GURWELL[1],
G. PETITPAS[1], M. RUPEN[2], K. D. ALEXANDER[1], E. M. LEVESQUE[11], C. FRANSSON[12], A. BRUNTHALER[13], M. F. BIETENHOLZ[14,15],
N. CHUGAI[16], J. GRINDLAY[1], A. COPETE[1], V. CONNAUGHTON[17], M. BRIGGS[17], C. MEEGAN[18], A. VON KIENLIN[19], X. ZHANG[19],
A. RAU[19], S. GOLENETSKII[20], E. MAZETS[20], AND T. CLINE[21]

[1] Harvard-Smithsonian Center for Astrophysics, 60 Garden St., Cambridge, MA 02138, USA
[2] National Radio Astronomy Observatory, Socorro, NM 87801, USA
[3] School of Natural Sciences, Institute for Advanced Study, Einstein Drive, Princeton, NJ 08540, USA
[4] Raymond and Beverly Sackler School of Physics & Astronomy, Tel Aviv University, Tel Aviv 69978, Israel
[5] Center for Research and Exploration in Space Science and Technology (CRESST), NASA Goddard Space Flight Center, Greenbelt, MD 20771, USA
[6] Department of Physics, University of Maryland, Baltimore County, 1000 Hilltop Circle, Baltimore, MD 21250, USA
[7] Department of Physics, Tokyo Institute of Technology, 2-12-1 Ohokayama, Meguro, Tokyo 152-8551, Japan
[8] Space Sciences Laboratory, University of California, 7 Gauss Way, Berkeley, CA 94720-7450, USA
[9] NASA Goddard Space Flight Center, Greenbelt, MD 20771, USA
[10] Astronomy Department, University of Virginia, Charlottesville, VA 22904, USA
[11] CASA, Department of Astrophysical and Planetary Sciences, University of Colorado 389-UCB, Boulder, CO 80309, USA
[12] Department of Astronomy, The Oskar Klein Centre, Stockholm University, 106 91 Stockholm, Sweden
[13] Max-Planck-Institute für extraterrestrische Physik, Giessenbachstraße, 85748 Garching, Germany
[14] Department of Physics and Astronomy, York University, Toronto, M3J 1P3, Ontario, Canada
[15] Hartebeesthoek Radio Observatory, P.O. Box 443, Krugersdorp 1740, South Africa
[16] Institute of Astronomy, RAS, Pyatnitskaya 48, Moscow 11917, Russia
[17] Physics Department, The University of Alabama in Huntsville, Huntsville, AL 35809, USA
[18] Universities Space Research Association, NSSTC, 320 Sparkman Drive, Huntsville, AL 35805, USA
[19] Max-Planck-Institut für extraterrestrische Physik, Giessenbachstrasse 1, 85748 Garching, Germany
[20] Ioffe Physical-Technical Institute of the Russian Academy of Sciences, St. Petersburg 194021, Russia
[21] Emeritus, NASA Goddard Space Flight Center, Code 661, Greenbelt, MD 20771, USA

ABSTRACT

We report the discovery and detailed monitoring of X-ray emission associated with the Type IIb SN 2011dh using data from the *Swift* and *Chandra* satellites, placing it among the best-studied X-ray supernovae (SNe) to date. We further present millimeter and radio data obtained with the Submillimeter Array, the Combined Array for Research in Millimeter-wave Astronomy, and the Expanded Very Large Array during the first three weeks after explosion. Combining these observations with early optical photometry, we show that the panchromatic data set is well described by non-thermal synchrotron emission (radio/mm) with inverse Compton scattering (X-ray) of a thermal population of optical photons. In this scenario, the shock partition fractions deviate from equipartition by a factor, $(\epsilon_e/\epsilon_B) \sim 30$. We derive the properties of the shock wave and the circumstellar environment and find a time-averaged shock velocity of $\overline{v} \approx 0.1c$ and a progenitor mass-loss rate of $\dot{M} \approx 6 \times 10^{-5}\ M_\odot\ \mathrm{yr}^{-1}$ (for an assumed wind velocity, $v_w = 1000\ \mathrm{km\ s}^{-1}$). We show that these properties are consistent with the sub-class of Type IIb SNe characterized by compact progenitors (Type cIIb) and dissimilar from those with extended progenitors (Type eIIb). Furthermore, we consider the early optical emission in the context of a cooling envelope model to estimate a progenitor radius of $R_* \approx 10^{11}$ cm, in line with the expectations for a Type cIIb SN. Together, these diagnostics are difficult to reconcile with the extended radius of the putative yellow supergiant progenitor star identified in archival *Hubble Space Telescope* observations, unless the stellar density profile is unusual. Finally, we searched for the high-energy shock breakout pulse using X-ray and gamma-ray observations obtained during the purported explosion date range. Based on the compact radius of the progenitor, we estimate that the shock breakout pulse was detectable with current instruments but likely missed due to their limited temporal/spatial coverage. Future all-sky missions will regularly detect shock breakout emission from compact SN progenitors enabling prompt follow-up observations with sensitive multi-wavelength facilities.

Key word: supernovae: individual (SN 2011dh)

Online-only material: color figures

1. INTRODUCTION

A key open question in the study of core-collapse supernovae (SNe) is the nature and diversity of their progenitor systems. High-resolution optical imaging of nearby galaxies has firmly established that the progenitors of Type IIP SNe are red supergiants (Smartt 2009), while pre-discovery imaging for Type II SNe 1987A (Gilmozzi et al. 1987), 1993J (Aldering et al. 1994), and 2005gl (Gal-Yam et al. 2007; Gal-Yam & Leonard 2009) point to a diverse set of massive stars. An alternative route to the nature of the progenitors is to obtain panchromatic follow-up observations within days of explosion. The shock breakout pulse and subsequent adiabatic cooling of the ejecta can yield information on the progenitor

---

size since the duration and energy of these signals scales with the size of the progenitor star (Colgate 1974; Ensman & Burrows 1992; Waxman et al. 2007; Chevalier & Fransson 2008; Katz et al. 2010; Nakar & Sari 2010). Complementary follow-up observations at radio, millimeter, and X-ray bands provide unique diagnostics on the shock wave velocity which scale inversely with the progenitor radius. The utility of such a multi-wavelength technique was demonstrated by the serendipitous X-ray discovery and comprehensive follow-up study of SN 2008D (Soderberg et al. 2008; Chevalier & Fransson 2008).

On May 31.893 UT amateur astronomer Amadee Riou discovered an optical transient in M51 ($d = 8.4 \pm 0.6$ Mpc; Feldmeier et al. 1997; see also Vinko et al. 2012). Multiple individuals and groups subsequently confirmed the transient using pre- and post-discovery imaging (Griga et al. 2011; Silverman et al. 2011). The Palomar Transient Factory (PTF; Law et al. 2009) reported a deep non-detection in pre-discovery data constraining the onset of the optical emission to be May 31.275–31.893 UT (Arcavi et al. 2011b). Based on an initial spectrum on June 3.3 UT, the transient was classified as a Type II SN, designated SN 2011dh (Silverman et al. 2011). Further spectroscopy revealed evidence for helium absorption features prompting the re-classification as Type IIb (Arcavi et al. 2011a; Marion et al. 2011).

A putative progenitor star has been identified in pre-explosion *Hubble Space Telescope* (*HST*) images with a spectral energy distribution consistent with a yellow supergiant (Maund et al. 2011; Van Dyk et al. 2011). The mass of the star is estimated to be between $M_{\rm ZAMS} \approx 13$ and $21\,M_\odot$, but temperature-dependent bolometric corrections, discrepancies between evolutionary tracks, and treatments of rotation should also be carefully considered (Drout et al. 2009). Based on the estimated luminosity and temperature of the object, the stellar radius is $R_* \approx 10^{13}$ cm (Prieto & Hornoch 2011). Both Maund et al. (2011) and Van Dyk et al. (2011) discuss the possibility that the yellow supergiant is instead the binary companion to the SN 2011dh progenitor star. In this scenario, the actual progenitor star would have had a smaller radius.

Recently, Chevalier & Soderberg (2010) proposed that SNe IIb may be divided into two sub-classes based on the radius and mass-loss history of the progenitor star and the properties of the shock wave. In this framework, compact progenitors ($R_* \sim 10^{11}$ cm) with modulated radio light curves and shock wave velocities of $\bar{v} \sim 0.1c$ are identified as SNe cIIb with members including SNe 2001ig (Ryder et al. 2004), 2003bg (Soderberg et al. 2006a), and 2008ax (Roming et al. 2009). Meanwhile, extended progenitors ($R_* \sim 10^{13}$ cm) with smooth radio light curves and slower shock waves are identified as SNe eIIb (e.g., SN 1993J; Bartel et al. 2002; Weiler et al. 2007). The modulated radio emission points to an unusual (perhaps episodic) mass loss that may be unique to SNe cIIb.

SN 2011dh showed an initial peak magnitude of $M_g \approx -16.5$ mag at $\Delta t \approx 1$ day since explosion before fading quickly (Arcavi et al. 2011b; Prieto et al. 2011). The SN then re-brightened at $\Delta t \approx 5$ days. The two light-curve components may be interpreted as cooling envelope emission followed by a re-brightening due to the radioactive decay of ^{56}Ni. Based on a comparison of the SN 2011dh light curve with that of SN 1993J and a photospheric temperature measurement, Arcavi et al. (2011b) proposed that SN 2011dh belongs to the Type cIIb class.

Here, we report the discovery and monitoring of X-ray emission associated with SN 2011dh and present radio- and mm-band detections from the first few weeks after explosion.

We show that the radio and X-ray properties are consistent with those of SNe cIIb and dissimilar from those of SNe eIIb, suggesting that the progenitor was compact at the time of explosion. This is supported by our modeling of the early cooling envelope emission, which points to a progenitor radius of $R_* \approx 10^{11}$ cm. Together, these diagnostics suggest that the putative yellow supergiant progenitor is instead a binary companion or unrelated to the SN. Finally, we present a detailed compilation of X-ray and gamma-ray observations from multiple satellites and instruments obtained during the purported explosion date range. We estimate that the shock breakout pulse was detectable with current high-energy instruments but likely missed due to their limited temporal/spatial coverage.

2. OBSERVATIONS

Following the optical discovery of SN 2011dh, we initiated a prompt panchromatic follow-up campaign to map the non-thermal properties of the ejecta.

2.1. Swift/XRT Observations

Thanks to multiple Target-of-Opportunity (ToO) requests, *Swift*/X-ray Telescope (XRT) promptly observed SN 2011dh on June 3.50, just ∼3 days after the explosion. As initially reported in Margutti & Soderberg (2011), we discovered a bright X-ray source (S/N ∼ 10) at coordinates, R.A.$_{\rm J2000} = 13^{\rm h}30^{\rm m}5^{\rm s}.18$, decl.$_{\rm J2000} = +47°10'11''.14$ (uncertainty $4''$ radius, 90% confidence) at $1''$ from the optical SN position. This data analysis reported here supersedes the preliminary analysis presented in the circulars; we find a count rate of ~0.015 counts s^{-1} for this first epoch. We analyzed 69 ks of archival pre-SN *Swift*/XRT observations and these data reveal no X-ray source at the SN position with a 3σ upper limit of 5.6×10^{-4} counts s^{-1}. This fact, coupled to the spatial coincidence of the SN, strongly suggests that the new source represents the X-ray counterpart to SN 2011dh (Figure 1).

Observations of SN 2011dh with *Swift* continued for the next several weeks. We retrieved and analyzed the XRT data from the HEASARC archive collected in the time period June 3 to July 3 UT (total exposure time of 137 ks). All XRT data were analyzed with the HEASOFT (version 6.10) software package and corresponding calibration files; standard filtering and screening criteria were applied. Due to the proximity of a nearby, steady X-ray source (Figure 1), we adopted a 12 pixel ($\sim28''$) extraction region centered on the optical position; for lower count rates (<0.0025 counts s^{-1}) we reduced the extraction region to a radius of 6 pixels to increase the signal-to-noise ratio (S/N) and eliminate contamination from a nearby faint source. The background was estimated from the pre-explosion *Swift*/XRT data to properly account for the contamination from the extended X-ray emission associated with M51. A spectrum extracted over June 3–17 UT can be modeled by an absorbed power law with photon index $\Gamma = 1.5 \pm 0.2$ (90% c.l.) assuming a Galactic foreground column density $N_{\rm H} = 1.81 \times 10^{20}$ cm^{-2} (Kalberla et al. 2005) and no intrinsic absorption ($\chi^2/{\rm dof} = 70.7/73$, P-val $= 0.56$). Alternatively, a thermal plasma spectral model with best-fitting temperature $kT = 7.5^{+9.7}_{-3.3}$ keV (90% confidence level (c.l.)) can adequately represent the data ($\chi^2/{\rm dof} = 68.8/73$, P-val $= 0.62$). Both models give an average unabsorbed flux of $F_X \approx 1.65 \times 10^{-13}$ erg cm^{-2} s^{-1} (0.3–8 keV) corresponding to a luminosity, $L_X \approx 2 \times 10^{39}$ erg s^{-1}.
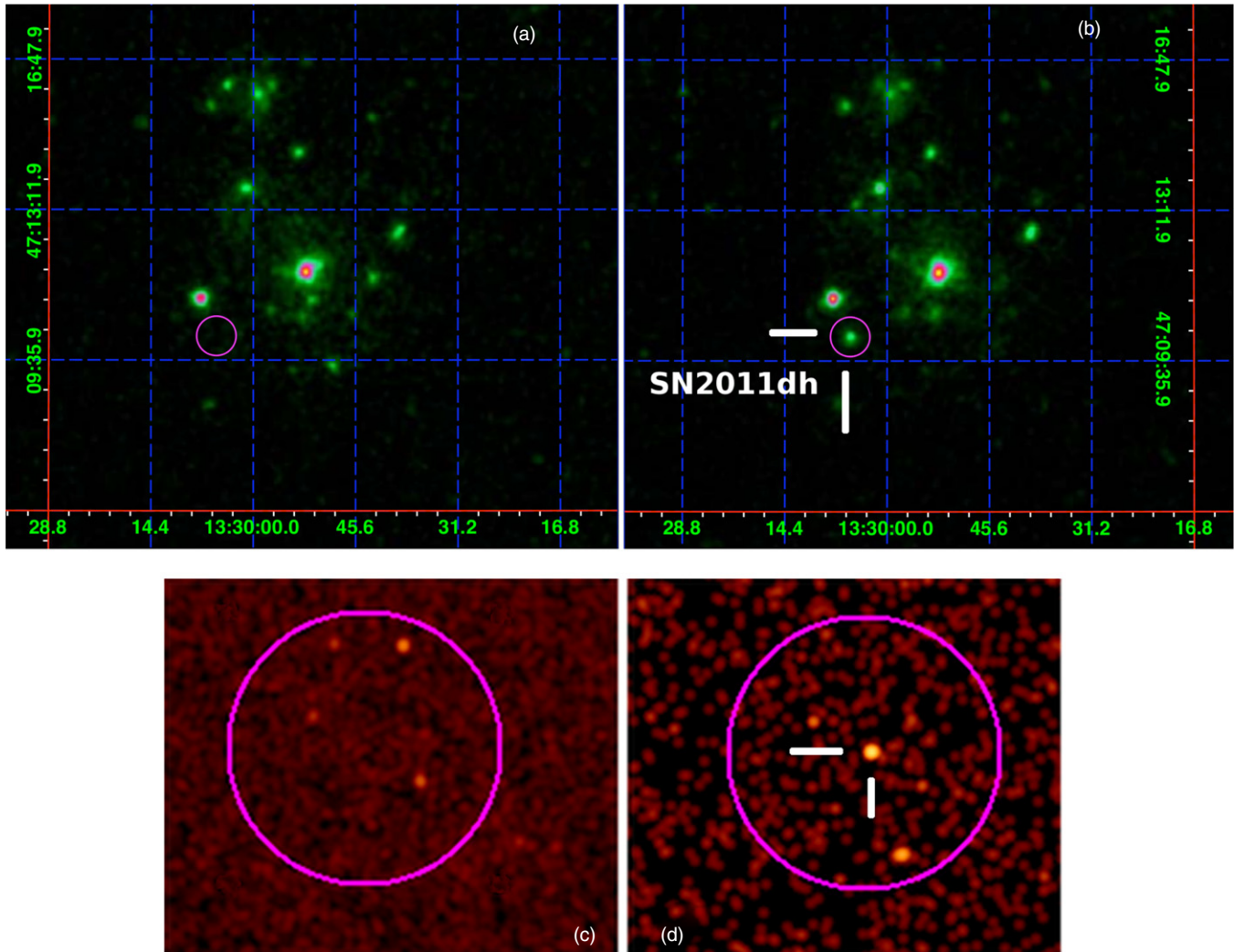
Figure 1. (a) A (0.3–10) keV co-added archival image (total exposure of 64 ks) of M51 obtained pre-explosion using *Swift*/XRT in the time range 2006 June to 2009 May. No statistically significant excess is detected at the SN2011dh position. (b) XRT observations of M51 (total exposure of 78 ks) obtained after the discovery of SN 2011dh clearly reveal an X-ray source at the SN position. (c) Archival *Chandra* observations reveal no source within 28 arcsec of the SN position (circle). (d) SN 2011dh is detected in our *Chandra* ToO observation on July 3. No bright contaminating X-ray sources are detected within the extraction region. We restrict our XRT extraction region at late times to avoid the faint source to the SW.

(A color version of this figure is available in the online journal.)

Our resulting X-ray light curve is shown in Figure 2 and Table 1. Over the first 10 days the SN faded by a factor ≈ 8. Adopting a simple power-law model for the decay, we derive an index of $\alpha = -0.8 \pm 0.2$ (90% c.l.). The source shows some evidence for spectral softening with time, with the photon index evolving from $\Gamma_1 = 0.9 \pm 0.3$ (90% c.l., $\Delta t = 3\text{--}7$ days) to $\Gamma_2 = 1.8 \pm 0.2$ (90% c.l., $\Delta t = 7\text{--}17$ days). In comparison with X-ray observations of SN 1993J, the softening observed for SN 2011dh begins at an earlier epoch.

2.2. Chandra Observations

We supplement our *Swift*/XRT light curve with two *Chandra* observations. As reported by Pooley (2011), SN 2011dh was observed with *Chandra* for 10 ks beginning on June 12.3 UT. The SN was detected with a count rate of $\sim$0.0115 counts s^{-1}. Adopting a power-law spectral model, they derive an X-ray flux of $F_X = (1.0 \pm 0.3) \times 10^{-13}$ erg cm^{-2} s^{-1} (0.5–8 keV).

On July 3.4 UT, we obtained a second 10 ks observation of SN 2011dh with the *Chandra* Advanced CCD Imaging Spectrometer (ACIS) under a ToO program (PI: Soderberg).

Data were reduced with the CIAO software package (version 4.3), with calibration database CALDB (version 4.4.2). We applied standard filtering using CIAO threads for ACIS data. We clearly detect a source at the SN position. Extracting within a 15 pixel aperture, we derive a (background-subtracted) count rate of $\sim$0.0049 counts s^{-1}. Adopting the same power-law spectral model described in Section 2.1, we derive an unabsorbed X-ray flux of $F_X = (2.75 \pm 0.55) \times 10^{-14}$ erg s^{-1} cm^{-2} (0.3–8 keV). We further note that we do not detect any bright nearby sources that would otherwise contaminate the extraction region adopted for the *Swift*/XRT data.

In Table 1 and Figure 2, we report the combined *Swift*/XRT and *Chandra* light curve of SN 2011dh, representing the best-sampled X-ray light curve for an SN IIb to date. We compare the X-ray properties of SN 2011dh with those of other SNe IIb including SNe 1993J (Chandra et al. 2009), 2001gd (Pérez-Torres et al. 2005), 2008ax (Roming et al. 2009), 2001ig (Schlegel & Ryder 2002), and 2003bg (Soderberg et al. 2006a). As is clear from the figure, the SN 2011dh X-ray light curve is more closely related to Type cIIb explosions and a factor of $\sim$10 less luminous than that observed for the Type eIIb SNe
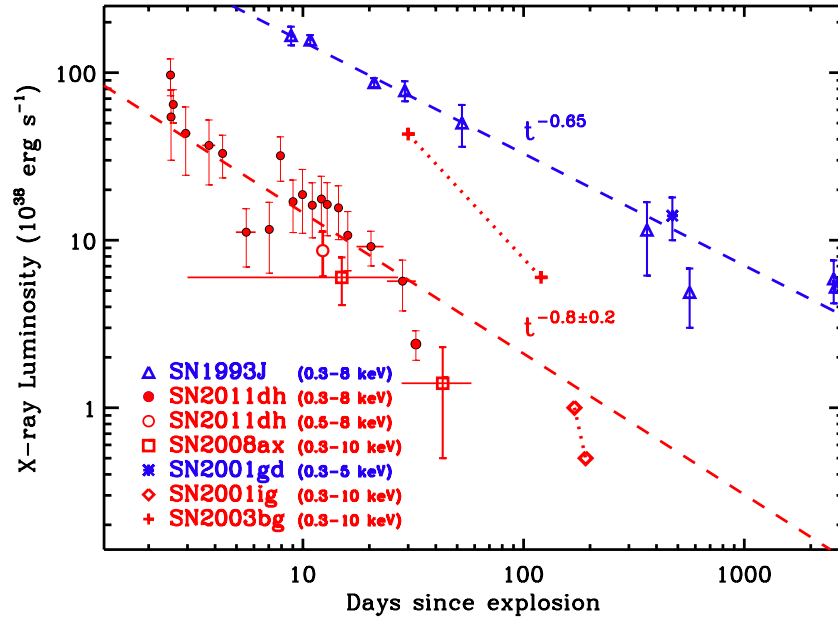
Figure 2. X-ray emission from SNe IIb: SN 1993J (Chandra et al. 2009), SN 2001gd (Pérez-Torres et al. 2005), SN 2008ax (Roming et al. 2009), SN 2001ig (Schlegel & Ryder 2002), and SN 2003bg (Soderberg et al. 2006a) and SN 2011dh (this work). Error bars are 1σ. For SN 2011dh, the energy band (0.3–8) keV is used to allow a direct comparison to SN 1993J. SNe of Type cIIb are shown in red while Type eIIb are shown in blue. The X-ray luminosities of Type cIIb appear lower than those of Type eIIb.

(A color version of this figure is available in the online journal.)

Table 1
X-Ray Observations of SN 2011dh

Date (UT)	Time Range (days)	Unabsorbed Flux[a] (erg cm^{-2} s^{-1})	Error (erg cm^{-2} s^{-1})	Satellite
June 3.512	0.004	1.12×10^{-12}	2.8×10^{-13}	*Swift*/XRT
June 3.526	0.003	6.28×10^{-13}	2.8×10^{-13}	*Swift*/XRT
June 3.585	0.007	7.45×10^{-13}	1.7×10^{-13}	*Swift*/XRT
June 3.943	0.152	5.01×10^{-13}	2.2×10^{-13}	*Swift*/XRT
June 4.753	0.252	4.25×10^{-13}	1.8×10^{-13}	*Swift*/XRT
June 5.326	0.033	3.80×10^{-13}	1.1×10^{-13}	*Swift*/XRT
June 6.536	0.571	1.29×10^{-13}	4.9×10^{-14}	*Swift*/XRT
June 8.042	0.181	1.34×10^{-13}	6.0×10^{-14}	*Swift*/XRT
June 8.911	0.253	3.69×10^{-13}	1.1×10^{-13}	*Swift*/XRT
June 10.020	0.301	1.96×10^{-13}	6.8×10^{-14}	*Swift*/XRT
June 10.954	0.165	2.16×10^{-13}	8.9×10^{-14}	*Swift*/XRT
June 12.027	0.370	1.87×10^{-13}	6.7×10^{-14}	*Swift*/XRT
June 13.127	0.179	2.03×10^{-13}	7.4×10^{-14}	*Swift*/XRT
June 13.887	0.200	1.89×10^{-13}	6.6×10^{-14}	*Swift*/XRT
June 15.493	0.601	1.80×10^{-13}	6.4×10^{-14}	*Swift*/XRT
June 16.969	0.136	1.23×10^{-13}	4.8×10^{-14}	*Swift*/XRT
June 21.345	2.848	1.06×10^{-13}	2.5×10^{-14}	*Swift*/XRT
June 29.278	4.227	6.57×10^{-14}	2.2×10^{-14}	*Swift*/XRT
June 12.300	0.115	1.00×10^{-13}	3.0×10^{-14}	*Chandra*/ACIS[b]
July 3.400	0.115	2.75×10^{-14}	5.5×10^{-15}	*Chandra*/ACIS

Notes.
[a] Energy range (0.3–8) keV.
[b] Observation reported by Pooley (2011) within energy range (0.5–8) keV.

1993J and 2001gd. We suggest that the Type cIIb sub-class *may* be further characterized by low X-ray luminosities and early spectral softening.

2.3. CARMA Observations

We observed SN 2011dh with the Combined Array for Research in Millimeter-wave Astronomy (CARMA; Bock

et al. 2006) beginning on 2011 June 4.1 UT. Observations were conducted with CARMA's nine 6.1 m antennas and six 10.4 m antennas in the D configuration, with a maximum baseline length of 150 m. We implemented radio and optical pointing (Corder et al. 2010). We selected central frequencies of $\nu = 107$ GHz and 230 GHz, with a total bandwidth of $\sim$6 GHz. Gain calibration was performed with J1153+495 and we used a source-calibrator cycle time of $\sim$15–20 minutes. Flux and bandpass calibration was carried out using observations of 3C273 and 3C345 and Neptune resulting in an overall uncertainty in the absolute flux calibration of $\sim$10%. We used the Multichannel Image Reconstruction Image Analysis and Display (MIRIAD; Sault et al. 1995) software package for data reduction. We integrated on SN 2011dh for 43 minutes at each frequency; a source is clearly detected at $\nu = 107$ GHz that is coincident with the optical and X-ray SN positions. Preliminary results for the $\nu = 107$ GHz observation were presented by Horesh et al. (2011b). Here, we present the results of the $\nu = 230$ GHz observation and a re-analysis of the $\nu = 107$ GHz data in which we have refined the flux calibration. Fitting a Gaussian model to the source, we derive an integrated flux density of $F_\nu = 4.5 \pm 0.3$ mJy at $\nu = 107$ GHz and a 3σ upper limit of $F_\nu \lesssim 3.5$ mJy at $\nu = 230$ GHz (Table 2). Thus, the radio spectrum is optically thin between the two millimeter (mm) bands at $\Delta t \approx 4$ days since explosion.

2.4. SMA Observations

Contemporaneously with the CARMA observations, we observed SN 2011dh with the Submillimeter Array (SMA; Ho et al. 2004) on June 4.0 UT in the compact configuration at a frequency of $\nu = 230$ GHz with 8 GHz bandwidth. Observations included all eight antennas. Passband calibration was performed in the standard way using Neptune, 3C454.3 and 3C279. We used 3C279 for flux calibration, verifying our calibration with observations of Titan in addition to 3C279 and our gain calibrators on June 10 UT. The absolute flux calibration is accurate

Table 2
Radio and Millimeter Observations of SN 2011dh

Date (UT)	Central Frequency (GHz)	Flux Density (mJy)	Error (mJy)	Telescope
June 4	22.5	2.68	0.10	EVLA[a]
...	107	4.5	0.3	CARMA
...	230	$\leqslant 3.5$	...	CARMA
...	230	3.6	0.9	SMA
June 17	5.0	2.430	0.037	EVLA
...	6.8	4.090	0.048	EVLA
...	8.4	5.535	0.057	EVLA
...	13.5	6.805	0.072	EVLA
...	16.0	6.721	0.070	EVLA
...	20.5	6.472	0.195	EVLA
...	25.0	5.127	0.155	EVLA
...	29.0	4.603	0.140	EVLA
...	36.0	3.473	0.108	EVLA

Note. [a] Observation reported by Horesh et al. (2011a).

to ∼10%. We flagged low elevation data ($<21°$) and the first several hours of the observation when weather conditions were less favorable, prior to improved pointing solutions, and when one antenna was missing. The data were calibrated using standard MIR/IDL routines developed for the SMA, with further calibration and imaging carried out in MIRIAD and the Astronomical Image Processing System (AIPS; Greisen 2003). The resulting total integration time on source was 2.75 hr. We detect a radio source coincident with the SN position with a flux density of $F_\nu = 3.6 \pm 0.9$ mJy (Table 2). This detection is not inconsistent with the 3σ upper limit from CARMA.

2.5. EVLA Observations

On June 4.25 UT, a radio counterpart was detected with the Expanded Very Large Array (EVLA; Perley et al. 2009) with a flux density of $F_\nu = 2.68 \pm 0.10$ mJy at $\nu = 22.5$ GHz (Horesh et al. 2011a). There is no coincident radio source in the catalog of M51 compact radio sources (Maddox et al. 2007). A comparison with the CARMA and SMA flux densities obtained contemporaneously indicates that the spectral peak lies between the EVLA and CARMA bands (Figure 3).

We began monitoring SN 2011dh with the EVLA on June 17 UT ($\Delta t \approx 17$ days after explosion) as part of a Rapid Response observing program for long-term monitoring of the SN (PI: Soderberg). Data were collected within the wide C, X, Ku, K, and Ka bands. Within each of these bands (except X), we selected two central frequencies enabling spectral coverage spanning $\nu = 5.0$–36.0 GHz. Each central frequency has associated bandwidth of 0.8–1.0 GHz. All observations were obtained in the (most extended) A-array. We used J1327+4326 to monitor the phase while the absolute flux calibration was carried out using 3C286. Data were reduced using AIPS and the Common Astronomy Software Applications. We fit a Gaussian model to the radio SN emission in each observation to derive the integrated flux density (Table 2). The reported flux density errors include errors from Gaussian fitting, the map rms noise, and systematic errors of 1% at low frequencies (5–16 GHz) and 3% at high frequencies (20.5–36.0 GHz). At this epoch, the peak of the radio spectrum has clearly shifted to the centimeter (cm) band.

Additional observations with EVLA are ongoing and are the focus of a follow-up paper (Krauss et al. 2012). In Figure 3, we compare the radio spectrum of SN 2011dh with the newly
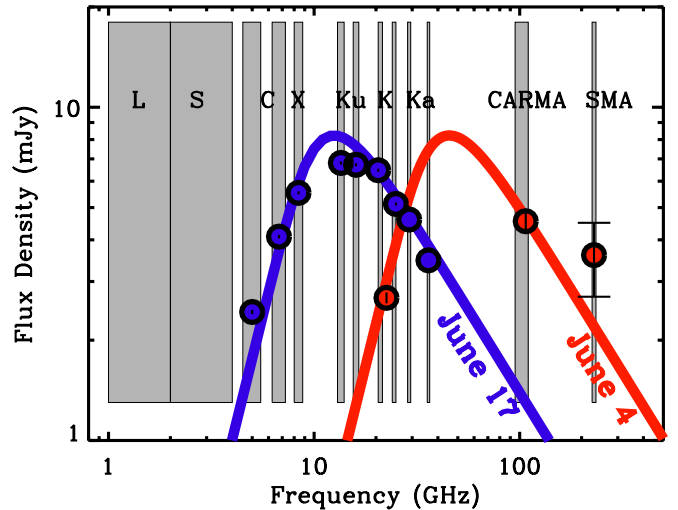

Figure 3. Radio spectrum of SN 2011dh across multiple epochs—$\Delta t \approx 4$ (red) and 17 (blue) days—is well described by a synchrotron self-absorbed spectral model with $F \propto \nu^{5/2}$ ($F_\nu \propto \nu^{-(p-1)/2}$) below (above) the spectral peak, ν_p. The observations indicate an electron energy index of $p \approx 3$. Error bars are 1σ. The gray bands mark the EVLA, CARMA, and SMA bands used in our long-term study of SN 2011dh as the spectral peak cascades to lower frequencies with time (see Krauss et al. 2012 for a detailed discussion).

(A color version of this figure is available in the online journal.)

available and unprecedented wide bands of EVLA which enable continuous spectral coverage from ∼1 to 40 GHz. SN 2011dh represents the first SN for which such detailed mapping of the spectrum has been possible in the EVLA era.

3. A MODEL FOR THE RADIO EMISSION

Early radio observations of SNe uniquely trace the shock wave as it races ahead of the bulk ejecta and shock-accelerates particles in the local circumstellar medium (CSM; Chevalier 1982). This environment was enriched by the progenitor star wind during the centuries leading up to the explosion. Through this dynamical interaction, the shock wave accelerates CSM electrons into a power-law distribution, $N(\gamma) \propto \gamma^{-p}$, above a minimum Lorentz factor, γ_m. The accelerated electrons gyrate in amplified magnetic fields giving rise to non-thermal synchrotron emission. In the case of Type Ibc and cIIb SNe, the radio emission is quenched at low frequencies primarily due to synchrotron self-absorption (SSA), producing a spectral turnover that defines the peak of the radio spectrum, ν_p. The self-absorbed radio spectrum is described by $F_\nu \propto \nu^{5/2}$ below ν_p and $F_\nu \propto \nu^{-(p-1)/2}$ above ν_p. As shown in Figure 3, our EVLA, CARMA, and SMA observations of SN 2011dh on two separate epochs are well described by a synchrotron self-absorbed spectrum with $p \approx 3$. We note that the modest disagreement between the SSA model and the measurements near the spectral peak may indicate asphericity of the emitting region (see Krauss et al. 2012 for a detailed discussion).

Chevalier (1998) showed that for radio SNe with minimal free–free absorption, the radius of the shock wave, R, and its time-averaged velocity, $\overline{v}$, can be robustly estimated from the observed values of ν_p and the associated peak spectral luminosity, $L_{\nu,p}$. As the shock wave decelerates, the optical depth to absorption processes declines and ν_p cascades to lower frequencies; for the case of free expansion, we expect $\nu_p \propto t^{-1}$ and a nearly constant peak spectral luminosity (Chevalier 1998). For $p \approx 3$, the shock wave radius is given by $R \approx 3.3 \times 10^{15} (\epsilon_e/\epsilon_B)^{-1/19} (L_{\nu_p,26})^{9/19} \nu_{p,5}^{-1}$ cm, where $L_{\nu_p,26}$
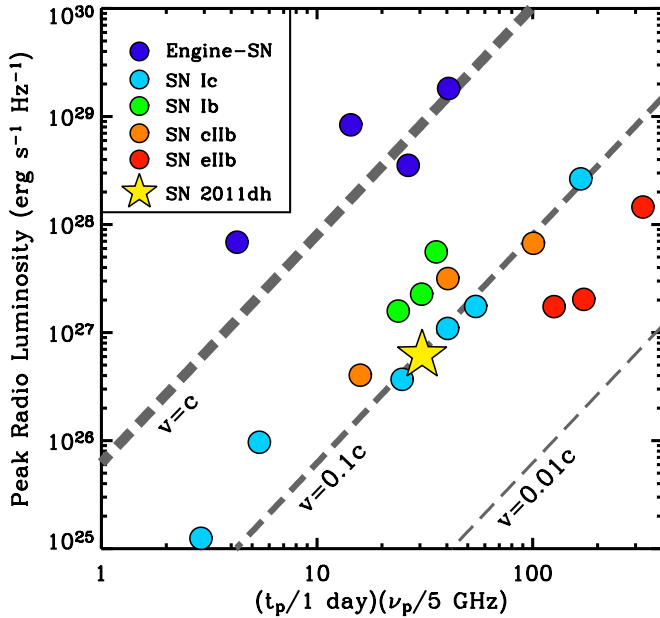
Figure 4. Radio properties of various SNe are compared including SNe Ib (green), Ic (cyan), cIIb (orange), eIIb (red), and engine-driven SNe associated with nearby gamma-ray bursts (blue). The properties of the spectral peak can be used to derive the shock wave velocity (dashed lines). With a blast wave velocity of $\overline{v} \approx 0.1c$, SN 2011dh (yellow star) is more similar to Types Ibc and cIIb than Type eIIb. Adapted from Chevalier & Soderberg (2010).

(A color version of this figure is available in the online journal.)

is normalized to 10^{26} erg s^{-1} Hz^{-1} and $\nu_{p,5}$ is normalized to 5 GHz (Chevalier & Fransson 2006). The fractions of post-shock energy density shared by accelerated electrons and amplified magnetic fields are denoted by ϵ_e and ϵ_B, respectively, and we assume that the radio-emitting region is half of the total volume enclosed by a spherical shock wave.

As shown in Figure 3, for SN 2011dh we find $\nu_p \approx 40$ and ≈ 11 GHz on 2011 June 4 and 17 ($\Delta t \approx 4$ and 17 days), respectively, with an associated peak luminosity of $L_{\nu_p,26} \approx 6.7$ on both epochs. These observables correspond to shock wave radii of $R \approx (1.0, 3.7) \times 10^{15}$ cm assuming typical partition values of $\epsilon_e = \epsilon_B = 0.1$. The time-averaged shock wave velocity is thus $R/\Delta t \approx \overline{v} \approx 0.1c$ and thus a factor of ~ 2 faster than the material at the optical photosphere at $\Delta t \approx 3$ days (Silverman et al. 2011). The total internal energy required to power the observed radio signal can be estimated from the post-shock magnetic energy density, $E = B^2 R^3/12\epsilon_B$. As shown by Chevalier & Fransson (2006), the amplified magnetic field is directly determined from the spectral properties, $B \approx 0.70(\epsilon_e/\epsilon_B)^{-4/19} L_{\nu_p,26}^{-2/19} \nu_{p,5}$ G. At $\Delta t \approx 4$ and 17 days, we find $B \approx 4.5$ and 1.2 G. The total internal energy is thus $E \approx (1.7, 6.3) \times 10^{46}$ erg for the two epochs, respectively, by maintaining the assumption that $\epsilon_B = 0.1$, i.e., $\epsilon_{B,-1}$. The roughly linear temporal increase of internal energy is consistent with a slightly decelerated shock wave. As shown in Figure 4, the shock wave properties of SN 2011dh are similar to those of Type cIIb, which tend to also be characterized by shock wave velocities of $\overline{v} \gtrsim 0.1c$ while slower shock waves are inferred for SNe eIIb.

The progenitor mass-loss rate is $\dot{M} \approx 0.39 \times 10^{-5} \epsilon_{B,-1}^{-1} (\epsilon_e/\epsilon_B)^{-8/19} L_{\nu_p,26}^{-4/19} \nu_{p,5}^2 t_{p,10}^2 M_\odot$ yr^{-1}, where $t_{p,10}$ is the observed time of the spectral peak normalized to 10 days and we have assumed a wind velocity of $v_w = 1000$ km s^{-1}. Thus,

we estimate a progenitor mass-loss rate for SN 2011dh of $\dot{M} \approx 3 \times 10^{-5} M_\odot$ yr^{-1}, similar to the mass-loss rates derived for SNe Ibc and cIIb and also similar to the values observed for Galactic Wolf–Rayet stars (Cappa et al. 2004; Crowther 2007), and a factor of 100 lower than the mass-loss rate inferred for SN 1993J (Fransson et al. 1996). We note that in this framework, the radio data constrain the ratio, $(\dot{M}/v_w)$, such that a variation in the assumed value of v_w shifts the mass-loss rate estimate by the same factor.

4. A MODEL FOR THE X-RAY EMISSION

On timescales of days after explosion, the X-ray emission observed from SNe Ibc and IIb may be dominated by a number of different emission processes including synchrotron, thermal, and inverse Compton (IC) scattering. Continued energy input from a compact remnant (black hole, magnetar) has also been invoked to explain the X-ray emission from some events (e.g., SN 2006aj, Mazzali et al. 2006; Soderberg et al. 2006b; SN 1979C, Patnaude et al. 2011). The temporal and spectral evolution of the radio and X-ray emission, together with their observed luminosity values, enables these different processes to be distinguished. Here, we consider the nature of the observed X-ray light curve for SN 2011dh.

The radio-to-X-ray spectral index is observed to be $\beta_{RX} \approx -0.7$ on both June 4 and 17 UT. Thus, an extrapolation of the optically thin radio synchrotron spectrum with $p \approx 3$ underestimates the X-ray flux at both epochs by a factor of ~ 140. Similarly high radio-to-X-ray spectral indices are not atypical for SNe Ibc and IIb (see Chevalier & Fransson 2006 and references within). Attributing the X-rays to synchrotron emission would require efficient particle acceleration and a flattening of the electron distribution at high energies.

As shown in Chevalier & Fransson (2003), the thermal emission from shock-heated ejecta in the reverse shock region may give rise to strong free–free X-ray emission. If the material is fully ionized and in temperature equilibrium, the expected luminosity is broadly determined by the electron temperature and the mass-loss rate of the progenitor star with an expected linear decay in time. We use Equations (25)–(30) of Chevalier & Fransson (2006) with $\overline{v} \approx 0.1c$ and $\dot{M} \approx 3 \times 10^{-5} M_\odot$ yr^{-1} to estimate the electron temperature.[23] The expected free–free X-ray luminosity for SN 2011dh is then $L_{\rm ff} \approx 2.5 \times 10^{37}$ erg s^{-1} on June 4 UT. This is a factor of ~ 200 lower than the *Swift*/XRT measurement at this epoch (Figure 2).

We next consider an IC scattering model in which the optical photons associated with both envelope cooling emission and the radioactive decay of ^{56}Ni are upscattered to the X-ray band by radio-emitting electrons (Chevalier et al. 2006). In this scenario, the X-ray decay should track the optical evolution through the cooling envelope decay to the re-brightening due to ^{56}Ni decay. The early optical emission indicates an average luminosity of $L_{\rm bol} \sim$ few $\times 10^{42}$ erg s^{-1} and a minimum near $\Delta t \approx 5$ days. The X-ray light curve suggests a similar minimum near this epoch and an overall decay of roughly $L_X \propto t^{-1}$ (Figure 2). Adopting the formalism of Chevalier & Fransson (2006) and assuming the relativistic electron population extends down to ($\gamma_m = 1$), the predicted IC emission is $L_{\rm IC} \approx 2.9 \times 10^{36} \epsilon_{B,-1} \dot{M}_{-5} (\epsilon_e/\epsilon_B)^{11/19} (v/0.1c)^{-1} L_{\rm bol,42} \Delta t_{d,10}^{-1}$ erg s^{-1}, where $\dot{M}_{-5}$ is the mass-loss rate normalized to $10^{-5} M_\odot$ yr^{-1}

---

[23] We note that Chevalier & Fransson (2006) adopt the notation $A_* \equiv A/(5 \times 10^{11}$ g cm$^{-1})$, where $A = \dot{M}/4\pi v_w$.

and we maintain the assumption of $v_w = 10^3$ km s^{-1}. Here, $\Delta t_{d,10}$ is the time since explosion normalized to 10 days.

We find that the X-ray emission may be attributed to IC emission if the assumption of equipartition is relaxed and $(\epsilon_e/\epsilon_B) \approx 30$ with $\epsilon_B \approx 0.01$. This deviation from equipartition implies modest adjustments to our physical parameter estimates, including a factor of ~ 2 increase in the mass-loss rate and a minimal increase in the inferred total internal energy of the radio-emitting material. The modified values for the mass-loss rate and magnetic field are $\dot{M}_{-5} \approx 6$ and $B \approx 2.2$ G, respectively. A prediction of this model is that the X-ray light curve will decay more steeply following the optical SN peak (Chevalier & Fransson 2006), which may be suggested by our *Chandra* measurement on July 3 UT.

5. CONSTRAINTS ON THE PROGENITOR SIZE

The early optical emission from SNe is dominated by the adiabatic cooling of envelope material following the breakout of the shock wave through the stellar surface (Ensman & Burrows 1992). This component cascades through the optical band in the first few days following explosion. The radius and temperature associated with this component may be roughly approximated as thermal (although see Nakar & Sari 2010 for a more comprehensive discussion of the spectral evolution) and used together with estimates for the bulk SN parameters (including the ejecta kinetic energy, E_K, and mass, M_{ej}) leads to a determination of the progenitor radius, R_*. Such techniques have been used to derive the progenitor radius of SNe 1987A (Ensman & Burrows 1992), 1999ex and 2008ax (Chevalier & Soderberg 2010), 2008D (Chevalier & Fransson 2008; Soderberg et al. 2008), in addition to SN 2006aj associated with XRF 060218 (Campana et al. 2006; Waxman et al. 2007). Here, we adopt the formalism of Chevalier & Fransson (2008) in which the temperature of the photosphere is given by $T_{ph} \approx 7800 E_{K,51}^{0.03} M_{ej,\odot}^{-0.04} R_{*,11}^{0.25} \Delta t_d^{-0.48}$ K and the photospheric radius is $R_{ph} \approx 3 \times 10^{14} E_{K,51}^{0.39} M_{ej,\odot}^{-0.28} \Delta t_d^{0.78}$ cm. Here we have normalized $E_{K,51}$ to 10^{51} erg, $M_{ej,\odot}$ to $M_{\odot}$, and $R_{*,11}$ to 10^{11} cm. Within this framework, it is assumed that the density and pressure profiles of the envelope are consistent with those of Matzner & McKee (1999), and that the bolometric luminosity decays as $L_{ph} \propto \Delta t_d^{-0.34}$.

We model the first few optical observations ($\Delta t \lesssim 5$ days) including the initial detection of $L_{ph} \approx 10^{42}$ erg s^{-1} on June 1.191 UT (Arcavi et al. 2011b). Silverman et al. (2011) report a photospheric velocity of $v_{ph} \approx 17{,}600$ km s^{-1} at $\Delta t \approx 3$ days after explosion implying a ratio of $(E_{K,51}/M_{ej,\odot}) \sim$ few. We estimate $R_{ph} \approx 5 \times 10^{14}$ cm and $T_{ph} \approx 8000$ K at $\Delta t \approx 1$ day. This is roughly consistent with the photospheric temperature derived from optical spectroscopy (Arcavi et al. 2011b) and implies a compact progenitor since $T_{ph} \propto R_{*,11}^{0.25}$. The high luminosity of the initial detection requires a ratio, $E_K/M_{ej} \sim$ few, in line with the ratio implied by the high photospheric velocity. Thus, the early optical emission points to a compact progenitor, similar to those of SNe Ibc and cIIb, and consistent with the earlier reported by Arcavi et al. (2011b) and the conclusions of Murphy et al. (2011) based on a study of the SN 2011dh environment.

We note, however, that the observed optical decay, $L \propto \Delta t_d^{-1}$, is significantly steeper than the model prediction. This may point to an irregular density profile near the stellar surface, perhaps associated with an unusual mass-loss ejection in the final stage of the progenitor's evolution. Such an irregular density profile
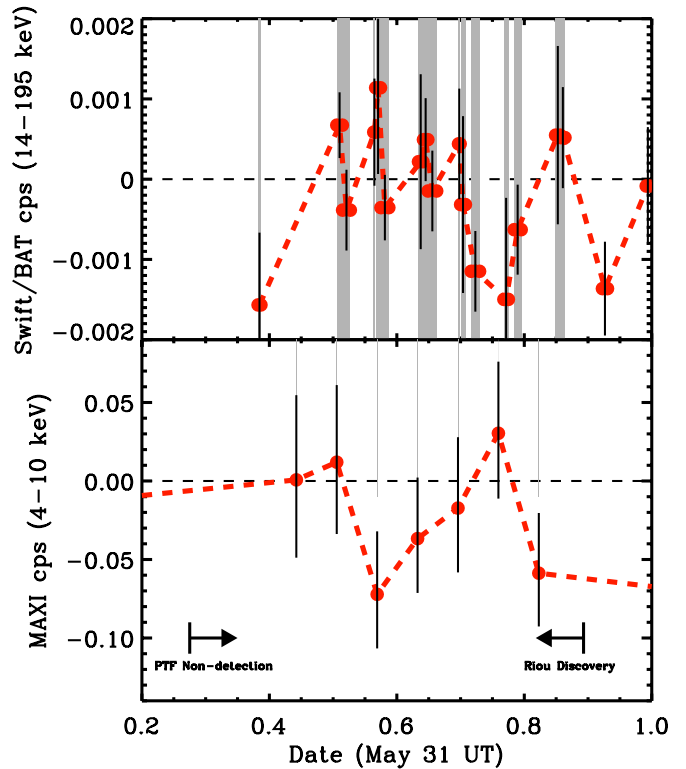

Figure 5. *Swift*/BAT (15–195 keV) and MAXI (4–10 keV) observations of the SN 2011dh field during the estimated explosion date range bounded by the discovery by Riou and pre-discovery limit (PTF) marked with arrows, May 31.275–31.893 UT (Arcavi et al. 2011b). No source is detected at the position of the SN during the individual ($\sim$1000 s) BAT pointings or ($\sim$80 s) MAXI scans. The time ranges when the SN was in the field of view of the instruments are shown in gray.

(A color version of this figure is available in the online journal.)

may affect some of the conclusions that we derived above based on the canonical model and this will be the focus of a future publication.

6. SHOCK BREAKOUT X-RAY EMISSION

For compact progenitors such as SN 2011dh, the breakout pulse may be detectable at X-ray and gamma-ray energies (e.g., SN 2008D; Soderberg et al. 2008). To this end, we searched for evidence of a high-energy pulse associated with the shock breakout of SN 2011dh using data collected by the *Swift* Burst Alert Telescope (BAT), the Monitor of All-sky X-ray Image (MAXI) camera attached to the *Japanese Experiment Module*, and the Interplanetary Network (IPN: Mars Odyssey, Konus-*Wind*, *RHESSI*, *INTEGRAL* (SPectrometer on *INTEGRAL*-Advanced Camera for Surveys), *Swift*/BAT, *Suzaku*, *AGILE*, and *Fermi*/Gamma-ray Burst Monitor (GBM); we note that *Messenger* was in superior conjunction and off during this period).

The position of SN 2011dh was observed by *Swift*/BAT over many pointings during the estimated explosion date range, May 31.275–31.893 UT. No gamma-ray emission was detected from the SN. We compile the *Swift*/BAT observations in Figure 5. Each pointing had a duration of $\sim$500–1000 s, and the total time on source was 11,148 s or 20% of the full explosion date range. We estimate the count rate at the SN position and also in the background in each pointing and note that the sensitivity varies as a function of the off-axis angle, ranging from 10 to 57 deg. Assuming a power-law spectrum for the breakout flux

with a photon index of $\Gamma = 2$, we infer 5σ upper limits on the gamma-ray emission from the SN of $F_\gamma \lesssim (1.1\text{--}3.9) \times 10^{-9}$ erg cm^{-2} s^{-1} (15–195 keV) for each individual pointing. The combined upper limit is $F_\gamma \approx 2.8 \times 10^{-10}$ erg cm^{-2} s^{-1} for the same energy range. At the distance of M51, this limit corresponds to a luminosity of $L_\gamma \lesssim 2.4 \times 10^{42}$ erg s^{-1}. We further note that no emission was detected by *Swift*/BAT in the direction of the SN during spacecraft slews throughout this time period; the BAT Slew Survey (Grindlay 2007) places a $\sim 4\sigma$ upper limit within energy range (15–50) keV.

MAXI (Matsuoka et al. 2009) is an X-ray all-sky monitor that scans most of the sky every 92 minutes with its Gas Slit Cameras (Mihara et al. 2011). Unfortunately, during the estimated period of the SN breakout, the direction of M51 was covered only by a camera with high background, resulting in less stringent limits than usual. The X-ray image taken at every scan transit (~ 80 s), encoded in one dimension by the detector position and the other by transit timing, was fitted to the point-spread function with the fixed source position to evaluate the source count rate. The energy range of (4–10) keV was chosen to maximize the S/N. Then the count rate was converted to energy flux assuming a power-law model with a photon index of $\Gamma = 2$ resulting in a conversion factor of $F_X \approx 1.1 \times 10^{-8}$ erg cm^{-2} s^{-1} (counts s^{-1})$^{-1}$. We derive an average 5σ upper limit of $L_X \lesssim 3.9 \times 10^{42}$ erg s^{-1}. In comparison, the observed breakout pulse from SN 2008D ($d \approx 30$ Mpc) had a luminosity ~ 25 times higher ($L_X \approx 10^{44}$ erg s^{-1}; 0.3–10 keV) with a duration of ~ 5 minutes.

While *Swift*/BAT and MAXI both have a limited temporal coverage, the IPN is full sky with temporal duty cycle of nearby 100%; it is sensitive to hard X-ray emission in the energy range (25–150) keV (Hurley et al. 2010). Within a two-day window centered on the estimated explosion date, a total of four triggered bursts were detected by the IPN. All four were confirmed through observations by multiple instruments or spacecrafts and thus could be localized. These detections include *Fermi*/GBM (three bursts), Konus (one), *INTEGRAL* (one), and *Swift*/BAT (one). In all cases the localizations were statistically *inconsistent* at a $\gtrsim 3\sigma$ level with the position of SN 2011dh. Thus, we find no evidence for a detected gamma-ray transient in coincidence with SN 2011dh and adopt an upper limit of $F_\gamma \lesssim 6 \times 10^{-7}$ erg cm^{-2} s^{-1} corresponding to an energy of $E_\gamma \lesssim 5 \times 10^{45}$ erg for SN 2011dh.

6.1. A Comparison to Breakout Predictions

Here, we compare theoretical predictions for a prompt breakout pulse with the available X-ray and γ-ray limits. We consider a model in which the progenitor is compact, $R_{*,11} \approx 1$, and embedded in a stellar wind with $\dot{M}_{-5} \approx 6$. In the standard SN Ibc model of Chevalier & Fransson (2006), also applicable to SNe cIIb, the shock wave radius evolves as $R \propto t^m$ with $m \approx 0.9$. Extrapolating back to the breakout radius, the shock wave speed at the stellar surface is $v_0 \approx 0.3c$ and we define $\beta_0 \approx 0.3\beta_{-0.5}$ as the shock velocity (divided by c) at this time. In the case of such fast shock velocities, there are deviations from thermal equilibrium resulting in high-energy emission (Katz et al. 2010; Nakar & Sari 2010; Sapir et al. 2011).

The optical depth at the stellar surface is $\tau = \kappa \dot{M}/4\pi v_w r \approx 2\dot{M}_{-5}R_{11}^{-1}$, where we adopt $\kappa = 0.4$ cm^2 g^{-1} and R_{11} is the shock radius normalized to 10^{11} cm. The shock breakout will occur outside of the star, within the stellar wind at a radius, $R_{\rm br} = \beta_0 \kappa \dot{M}/4\pi v_w \approx 6 \times 10^{10}\dot{M}_{-5}\beta_{-0.5}$ cm as long as $R_* < R_{\rm br}$.

In the case of SN 2011dh, we therefore predict a wind breakout at radius, $R_{\rm br} \approx 4 \times 10^{11}$ cm. The energy associated with breakout is $E_{\rm br} \approx 3 \times 10^{43}\dot{M}_{-5}^2\beta_{-0.5}^3$ (Katz et al. 2012). On the breakout timescale, a radiative collisionless shock forms and an additional comparable or larger amount of energy is emitted (Katz et al. 2012). Adopting our parameters for SN 2011dh, we predict $E_{\rm br} \gtrsim 10^{45}$ erg. During the transition from a radiation-mediated shock to collisionless, the temperature rises steadily from $\gtrsim$ keV to $\gtrsim 100$ keV and we roughly estimate the spectrum to be $\nu F_\nu \sim$ constant.

The predicted breakout energy is within the detectability range of the *Swift*/BAT and MAXI upper limits spanning (4–195) keV, however, both offer only limited temporal coverage. We estimate the rise time of the breakout pulse to be $t_{\rm br} \approx R_{\rm br}/v_0 \approx 1$ minute. Efficient emission from the collisionless shock continues beyond this time, and the full duration of the pulse is necessarily longer. Given the large gaps in the *Swift*/BAT and MAXI coverage (see Figure 5), especially toward the beginning of the explosion date range, we speculate that *Swift* and MAXI missed the breakout pulse. The IPN upper limit is a factor of a few above the predicted energy and thus consistent with this breakout model. Finally, we note that if the progenitor was more extended with a radius, $R_* \approx 10^{13}$ cm, a stronger pulse of $E_{\rm br} \sim 3 \times 10^{47}R_{*,13}^2$ erg is expected at lower frequencies, $h\nu \lesssim 300$ eV. Such a pulse is not constrained by the hard X-ray/gamma-ray observations presented here.

7. CONCLUSIONS

We present multi-wavelength follow-up observations of SN 2011dh spanning the radio, millimeter, X-ray, and gamma-ray bands and obtained within the first few seconds to weeks following the explosion. The X-ray light curve for SN 2011dh is perhaps the best-sampled to date for an SN IIb and suggests that X-ray properties (luminosity, spectral evolution) may further distinguish compact and extended progenitors. Using the newly available wide bands of the EVLA, we show that the radio and millimeter data are consistent with a synchrotron self-absorbed spectrum, while the X-ray emission may be understood as IC upscattering of optical SN photons assuming a non-negligible deviation from equipartition of the shock partition fractions. These data offer unique diagnostics (shock wave velocity, $\bar{v} \approx 0.1c$) and point to a compact progenitor star. Through modeling of the early optical emission, we find that the photosphere is characterized by a low temperature, $T_{\rm ph} \approx 8000$ K, and the physical parameters of the ejecta are constrained to be $E_{K,51}/M_{\rm ej,\odot} \sim$ few. These properties point to a compact progenitor, $R_* \approx 10^{11}$ cm, however, we find that the fast decay of the early optical emission at $\Delta t \lesssim 5$ day is incompatible with canonical cooling envelope models and may suggest an irregular ejecta profile. A compact progenitor size appears inconsistent with the extended radius ($R_* \sim 10^{13}$ cm) of the coincident yellow supergiant identified in pre-explosion *HST* imaging, suggesting an unusual density profile for the outer layers of the progenitor star. It may be possible to explain the coincident object as a binary companion, however, it is estimated that the yellow supergiant phase lasts just ~ 3000 years (Drout et al. 2009) making this scenario improbable. At the same time, the rarity of yellow supergiants makes a positional coincidence unlikely, suggesting the supergiant is indeed related to the progenitor system.

If the supergiant was characterized by a low-mass envelope and a low-density stellar wind, it may be possible to reconcile

the radio and X-ray observations with the putative progenitor. Georgy (2012) recently suggested that the mass-loss rates for yellow supergiants have been theoretically overestimated. However, the early cooling envelope emission requires a substantially lower density envelope then those associated with supergiants; in this scenario, ejecta asymmetries may be the only way to reconcile the early optical data with the coincident supergiant as the progenitor.

We conclude that SN 2011dh is likely a member of the Type cIIb class of core-collapse explosions. Our long-term EVLA monitoring observations will reveal if the radio light curves are modulated (see Krauss et al. 2012 for details), indicative of a variable and/or episodic mass-loss history in the decades leading up to explosion—an observational characteristic shared by other SNe cIIb. In addition, our long-term monitoring with the Very Long Baseline Interferometer will provide a direct measurement of the shock radius and, in turn, an independent constraint on the shock partition fractions (Marti-Vidal et al. 2011; Bietenholz et al. 2012). Future observations of the explosion site with *HST* imaging will reveal whether the supergiant has disappeared, thereby directly linking it to the explosion.

Finally, we used the parameters derived above for the shock wave and progenitor to estimate that the shock breakout pulse from SN 2011dh was detectable in the X-ray and gamma-ray bands with current satellites. We attribute the lack of a detection as likely due to limited temporal/spatial coverage during the estimated explosion date. Looking forward, sensitive and wide-field X-ray experiments such as LOBSTER and JANUS will regularly discover shock breakout emission from similarly nearby and compact SN progenitors (see, e.g., Soderberg et al. 2009 for a discussion). Such detections will not only provide information on the progenitor size since the explosion date estimates will enable statistically significant searches for gravitational wave and neutrino counterparts (Ott 2009; Katz et al. 2012). Furthermore, these prompt discoveries will enable rapid low-frequency follow-up with sensitive radio and millimeter facilities thanks to the advent of EVLA, the Atacama Large Millimeter Array, ASKAP, and MeerKAT.

REFERENCES

Aldering, G., Humphreys, R. M., & Richmond, M. 1994, AJ, 107, 662
Arcavi, I., Gal-Yam, A., Polishook, D., et al. 2011a, ATel, 3413, 1
Arcavi, I., Gal-Yam, A., Yaron, O., et al. 2011b, ApJ, 742, L18
Bartel, N., Bietenholz, M. F., Rupen, M. P., et al. 2002, ApJ, 581, 404
Beitenholz, M. F., Brunthaler, A., Soderberg, A. M., et al. 2012, ApJ, in press (arXiv:1201.0771)
Bock, D. C.-J., Bolatto, A. D., Hawkins, D. W., et al. 2006, Proc. SPIE, 6267, 626713
Campana, S., Mangano, V., Blustin, A. J., et al. 2006, Nature, 442, 1008
Cappa, C., Goss, W. M., & van der Hucht, K. A. 2004, AJ, 127, 2885
Chandra, P., Dwarkadas, V. V., Ray, A., Immler, S., & Pooley, D. 2009, ApJ, 699, 388
Chevalier, R. A. 1982, ApJ, 258, 790
Chevalier, R. A. 1998, ApJ, 499, 810
Chevalier, R. A., & Fransson, C. 2003, in Supernovae and Gamma-Ray Bursters, ed. K. Weiler (Lecture Notes in Physics, Vol. 598; Berlin: Springer), 171
Chevalier, R. A., & Fransson, C. 2006, ApJ, 651, 381
Chevalier, R. A., & Fransson, C. 2008, ApJ, 683, L135
Chevalier, R. A., Fransson, C., & Nymark, T. K. 2006, ApJ, 641, 1029
Chevalier, R. A., & Soderberg, A. M. 2010, ApJ, 711, L40
Colgate, S. A. 1974, ApJ, 187, 333
Corder, S. A., Wright, M. C. H., & Carpenter, J. M. 2010, Proc. SPIE, 7733, 77333P
Crowther, P. A. 2007, ARA&A, 45, 177
Drout, M. R., Massey, P., Meynet, G., Tokarz, S., & Caldwell, N. 2009, ApJ, 703, 441
Ensman, L., & Burrows, A. 1992, ApJ, 393, 742
Feldmeier, J. J., Ciardullo, R., & Jacoby, G. H. 1997, ApJ, 479, 231
Fransson, C., Lundqvist, P., & Chevalier, R. A. 1996, ApJ, 461, 993
Gal-Yam, A., & Leonard, D. C. 2009, Nature, 458, 865
Gal-Yam, A., Leonard, D. C., Fox, D. B., et al. 2007, ApJ, 656, 372
Georgy, C. 2012, A&A, 538, L8
Gilmozzi, R., Cassatella, A., Clavel, J., et al. 1987, Nature, 328, 318
Greisen, E. W. 2003, in Information Handling in Astronomy - Historical Vistas, ed. A. Heck (Astrophysics and Space Science Library, Vol. 285; Dordrecht: Kluwer), 109
Griga, T., Marulla, A., Grenier, A., et al. 2011, CBET, 2736, 1
Grindlay, J. E. 2007, in ASP Conf. Ser. 373, The Central Engine of Active Galactic Nuclei, ed. L. C. Ho & J.-W. Wang (San Francisco, CA: ASP), 711
Ho, P. T. P., Moran, J. M., & Lo, K. Y. 2004, ApJ, 616, L1
Horesh, A., Stockdale, C., Frail, D. A., et al. 2011a, ATel, 3411, 1
Horesh, A., Zauderer, A., & Carpenter, J. 2011b, ATel, 3405, 1
Hurley, K., Golenetskii, S., Aptekar, R., et al. 2010, in AIP Conf. Ser. 1279, Deciphering the Ancient Universe with Gamma-ray Bursts, ed. N. Kawai & S. Nagataki (Melville, NY: AIP), 330
Kalberla, P. M. W., Burton, W. B., Hartmann, D., et al. 2005, A&A, 440, 775
Katz, B., Budnik, R., & Waxman, E. 2010, ApJ, 716, 781
Katz, B., Sapir, N., & Waxman, E. 2012, ApJ, 747, 147
Krauss, M. I., Soderberg, A. M., Chomiuk, L., et al. 2012, ApJ, in press (arXiv:1201.0770)
Law, N. M., Kulkarni, S. R., Dekany, R. G., et al. 2009, PASP, 121, 1395
Maddox, L. A., Cowan, J. J., Kilgard, R. E., Schinnerer, E., & Stockdale, C. J. 2007, AJ, 133, 2559
Margutti, R., & Soderberg, A. 2011, ATel, 3400, 1
Marion, G. H., Kirshner, R., Wheeler, J. C., et al. 2011, ATel, 3435, 1
Marti-Vidal, I., Tudose, V., Paragi, Z., et al. 2011, A&A, 535, L10
Matsuoka, M., Kawasaki, K., Ueno, S., et al. 2009, PASJ, 61, 999
Matzner, C. D., & McKee, C. F. 1999, ApJ, 510, 379
Maund, J. R., Fraser, M., Ergon, M., et al. 2011, ApJ, 739, L37
Mazzali, P. A., Deng, J., Nomoto, K., et al. 2006, Nature, 442, 1018
Mihara, T., Nakajima, M., Sugizaki, M., et al. 2011, PASJ, 63, 623
Murphy, J. W., Jennings, Z. G., Williams, B., et al. 2011, ApJ, 742, L4
Nakar, E., & Sari, R. 2010, ApJ, 725, 904
Ott, C. D. 2009, Class. Quantum Gravity, 26, 063001
Patnaude, D. J., Loeb, A., & Jones, C. 2011, New Astron., 16, 187
Pérez-Torres, M. A., Alberdi, A., Marcaide, J. M., et al. 2005, MNRAS, 360, 1055
Perley, R., Napier, P., Jackson, J., et al. 2009, Proc. IEEE, 97, 1448
Pooley, D. 2011, ATel, 3456, 1
Prieto, J. L., & Hornoch, K. 2011, ATel, 3433, 1
Prieto, J. L., Szczygiel, D. M., Pojmanski, G., & Beacom, J. F. 2011, ATel, 3432, 1
Roming, P. W. A., Pritchard, T. A., Brown, P. J., et al. 2009, ApJ, 704, L118
Ryder, S. D., Sadler, E. M., Subrahmanyan, R., et al. 2004, MNRAS, 349, 1093
Sapir, N., Katz, B., & Waxman, E. 2011, ApJ, 742, 36

Sault, R. J., Teuben, P. J., & Wright, M. C. H. 1995, in ASP Conf. Ser. 77, Astronomical Data Analysis Software and Systems IV, ed. R. A. Shaw, H. E. Payne, & J. J. E. Hayes (San Francisco, CA: ASP), 433

Schlegel, E. M., & Ryder, S. 2002, IAU Circ., 7913, 1

Silverman, J. M., Filippenko, A. V., & Cenko, S. B. 2011, ATel, 3398, 1

Smartt, S. J. 2009, ARA&A, 47, 63

Soderberg, A., Grindlay, J. E., Bloom, J. S., et al. 2009, Astro2010: The Astronomy and Astrophysics Decadal Survey, Science White Papers, 278

Soderberg, A. M., Berger, E., Page, K. L., et al. 2008, Nature, 453, 469

Soderberg, A. M., Chevalier, R. A., Kulkarni, S. R., & Frail, D. A. 2006a, ApJ, 651, 1005

Soderberg, A. M., Kulkarni, S. R., Nakar, E., et al. 2006b, Nature, 442, 1014

Van Dyk, S. D., Li, W., Cenko, S. B., et al. 2011, ApJ, 741, L28

Vinko, J., Takats, K., Szalai, T., et al. 2012, A&A, 540, 93

Waxman, E., Mészáros, P., & Campana, S. 2007, ApJ, 667, 351

Weiler, K. W., Williams, C. L., Panagia, N., et al. 2007, ApJ, 671, 1959